Study of premature quench fields of Nitrogen-doped Niobium cavities

Supervisor: Martina Martinello
Co-Supervisor: Mattia Checchin
Fermi National Accelerator Laboratory
Technical Division

Bianca Giaccone
University of Milan

October 16, 2017

1 Premise

My work during the internship focused on the study of the premature quench of the nitrogen doped cavities.
To study this phenomenon we tested two superconductive radio-frequency nitrogen doped cavities at 1.5 K and 2 K. After the RF tests we analyzed them with optical inspection and we analyzed cavities' replicas with laser confocal microscopy. We also used a SEM to study samples of nitrogen doped niobium.

During the first weeks of my internship, the vertical test facility at FNAL was in shutdown and we couldn't start immediately with the RF tests. My supervisor provided me with the data collected during the RF tests of one SRF 1.3 GHz cavity. This cavity had been tested both before and after the doping treatment, and had been measured with the same set-up that we would have later used for our RF tests. I analyzed the data of this cavity so that I would know how analyze the data of our RF tests.
Once the shutdown ended, I observed the RF tests of three LCLS II cavities and learned how the RF measurement system works.

I then took part to our RF tests, both during the preparation stages of the measurement, both during the measurement itself.
I was taught how to perform an optical inspection and then I proceeded with the optical inspection of the cavities.
I was taught how to use the optical microscope and then I studied the replicas with the confocal laser scanning microscopy.
I was taught how to use a SEM and then I used it to collect images of the samples.

2 Introduction

Nitrogen doping treatment was discovered in 2012 at FNAL. This treatment is performed on resonant superconducting cavities in order to enhance their quality factor: N-doping allows niobium cavities to reach quality factor up to three times higher than a standard processed cavity.
This happens thanks to a reduction of R_{BCS}, the BCS term in the surface resistance: the BCS term decreases with the accelerating field, instead of growing with E_{acc} as it happens in the non-doped cavities. The reduction of the BCS term causes an "anti-Q-slope" for medium values of the accelerating field. Figure (1a) shows the comparison between the quality factor of a doped cavity and a 120° baked, non-doped cavity.

However it has been observed that N-doped cavities quench at lower values of the accelerating field, compared with non-doped cavities. Quench means that the cavity reaches the critical temperature (for the niobium $T_c = 9.25\,\mathrm{K}$), or the critical magnetic field H_{c1} and passes from a superconductive state to normalconductive.
My internship work is focused on the study of the premature quench field of Nb N-doped cavities.
There are two main hypothesis to explain the premature quench of the N-doped cavities:

- the magnetic field enhancement due to surface asperities combined with the lowered critical field H_{c1} caused by the doping;

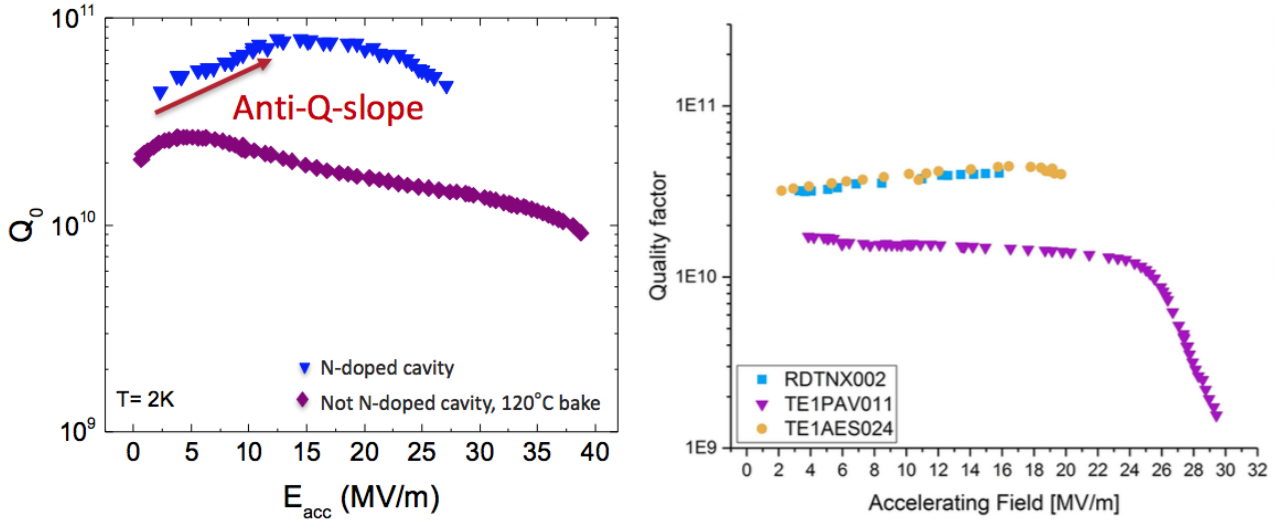

(a) (b)

Figure 1: Figure (a) shows the comparison between a N-doped and a non doped cavity. The nitrogen doped cavity shows an anti-Q-slope, in opposition to the Q-slope of the non-doped cavity. Figure (b) shows the results of the RF tests we measured on three cavities, one non-doped (TE1PAV011) and two N-doped with the "2/6" recipe (RDTNX002 and TE1AES024).

- the proximity break-down of possible niobium nitride phases at the surface survived to the post-doping EP.

Thanks to the advantages introduced by this treatment, it has been decided to use nitrogen-doped cavities in the LCLS upgrade. LCLS II will accelerate electrons in order to produce a X-ray FEL with a beam 10^4 times brighter and $8 \cdot 10^3$ times faster than the first one. LCLS II is using cavities made with niobium by two different vendors, Ningxia and Tokyo Denkai, and it has been discovered that statistically they show a different behaviour, as shown in figure (2).

For this reason we decided to test two single cell 1.3 GHz cavities, made from these two different vendors and doped with the same recipe, in order to study the premature quench field of nitrogen doped cavities. We also decided to perform surface analyses on samples treated with the same recipe and made with Ningxia and Tokyo Denkai niobium.

3 Accelerating cavities and nitrogen doping treatment

3.1 Accelerating SRF cavities

Resonating cavities are one of the key components of particle accelerators and one of their most important characteristic is the quality factor Q_0. The quality factor is defined as the ratio between the energy stored in the cavity and the energy lost in one period:

$$Q_0 = \frac{\omega_0 U}{P_c} \quad . \tag{1}$$

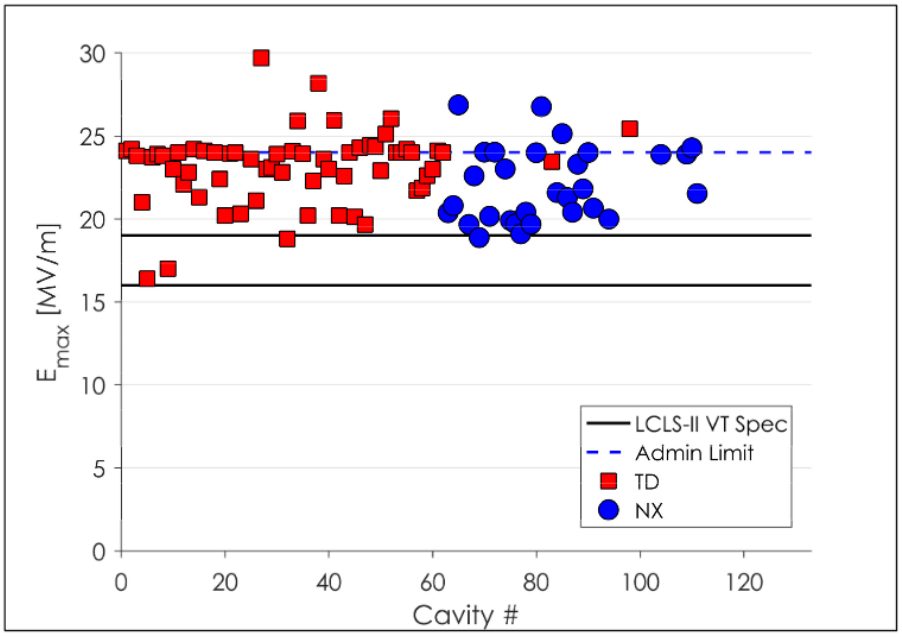

Figure 2: Comparison between Tokyo Denkai and Ningxia cavities. The dotted line is the administration limit set for the tests. Tokyo Denkai cavities appear to reach this value more easily than Ningxia cavities.

Knowing that the energy lost in one period due to the Joule effect is:

$$P_c = \frac{1}{2}\int_S R_s |\vec{H}|^2 ds \quad , \tag{2}$$

and

$$U = \frac{1}{2}\mu_0 \int_V |\vec{H}|^2 dv \quad , \tag{3}$$

we can write Q_0 as:

$$Q_0 = \omega_0 \mu_0 \frac{\int_V |\vec{H}|^2 dv}{\int_S R_s |\vec{H}|^2 ds} = \frac{G}{R_s} \quad . \tag{4}$$

Here G is the geometric factor of the resonant cavity and its value is $270\,\Omega$, and R_s is the surface resistance.

Using the π-mode to accelerate particles we have that

$$E_{acc} = \frac{V}{L} = \frac{1}{L}\left| \int E_z\,(r=0,z)\, e^{i\omega_0 z/c} dz \right| . \tag{5}$$

We can use the shunt impedance R_a to re-write the expression for E_{acc}. Knowing that

$$R_a = \frac{V_{acc}^2}{P_c} \quad , \tag{6}$$

and using the definition of quality factor we have

$$\left[\frac{R_a}{Q}\right] = \frac{V^2}{\omega_0 U} \quad , \tag{7}$$

and its usual value for the TM_{010} mode is $196\,\Omega$. We can write E_{acc} as:

$$E_{acc} = \frac{1}{L}\sqrt{\left[\frac{R_a}{Q}\right] Q_0\, P_c} \quad . \tag{8}$$

3.2 Surface Resistance

"The Q-factor is determined by the cavity RF surface resistance R_s: $Q0 = G/R_s$, where $G = 270\,\Omega$ is the geometrical factor which is independent on material properties. The RF surface resistance can be decomposed in two contributions, one temperature dependent called BCS surface resistance (R_{BCS}) and one temperature independent called residual resistance (R_{res}). [...]

The BCS surface resistance was defined by Mattis and Bardeen. Based on the Bardeen-Cooper-Schrieffer theory of superconductivity, R_{BCS} decays exponentially with the temperature and depends on several material parameters, such as London penetration depth λ_L, coherence length ξ_0, energy gap Δ, critical temperature T_c, and mean free path l. Of most interest here is that from the Mattis-Bardeen calculation, R_{BCS} as a function of the mean free path shows a minimum around $\xi_0/2$.

It is well known that nitrogen-doping affects the BCS contribution which, in contrary of what happens with standard treatments, decreases with accelerating field. This results in an increasing of Q-factor with accelerating field called anti-Q-slope. The mechanisms that govern the anti-Q- slope are not well understood yet, even though some theories have been proposed. [...]

We define R_{res} as the sum of the two terms: the trapped flux residual resistance, R_{fl}, and the "intrinsic" residual resistance, R_0, in order to distinguish the effect of trapped flux from other contributions; therefore,

$$R_s(T, B_{trap}) = R_{BCS}(T) + R_{fl}(B_{trap}) + R_0 \tag{9}$$

where T is the temperature and B_{trap} is the trapped field.
Since at very low temperatures, R_{BCS} becomes negligible, the Q-factor is measured at 1.5 K, and the residual resistance is calculated as $R_{res} = G/Q(1.5\,\mathrm{K})$. If during the cooldown, the amount of trapped flux is minimized, then $R_{fl} \approx 0$ and $R_{res} \approx R_0$." [2]

R_{BCS} can be estimated as:

$$R_{BCS}(2\,\mathrm{K}) = R_s(2\,\mathrm{K}) - R_0 \quad , \tag{10}$$

if $R_{res} \approx R_0$; otherwise:

$$R_{BCS}(2\,\mathrm{K}) = R_s(2\,\mathrm{K}) - R_{res}(1.5\,\mathrm{K}) \quad . \tag{11}$$

3.3 Nitrogen doping

Nitrogen doping treatment consists in different steps.
"For the doping treatment, niobium cavities are typically treated with 800 °C degassing in HV for 2-3 hours, followed by injection of niotrogen (N_2) at high temperature. The N_2 flow is set to a specific partial pressure for a certain amount of time. During this step nitrogen reacts with the niobium at the surface and diffuses inside. After that, it is possible to perform a second, optional, step in which the cavity is maintained at high temperature, without nitrogen, in order to promote the diffusion of the nitrogen atoms inside the bulk, smoothing the concentration profile. Then, the heating is shut off and the cavity is let cooling till room temperature." [3]

The recipe now used for the nitrogen doping is known as "2/6": the cavity is baked at 800 °C for 2 minutes with nitrogen at 25 mTorr and then it undergoes 6 minutes of annealing. After the baking, the cavity is electropolished with a removal of 5 µm. This last step is important to remove the normalconducting NbN phases on the surface of the cavity, because they would affect the performance of the cavity causing a decrease of Q_0. After 5 µm of EP, only the interstitial nitrogen remains in the niobium. Nitrogen atoms absorbed as interstitial impurities in the niobium lattice increase the quality factor, thanks to the reduction of the BCS surface resistance with the accelerating field.

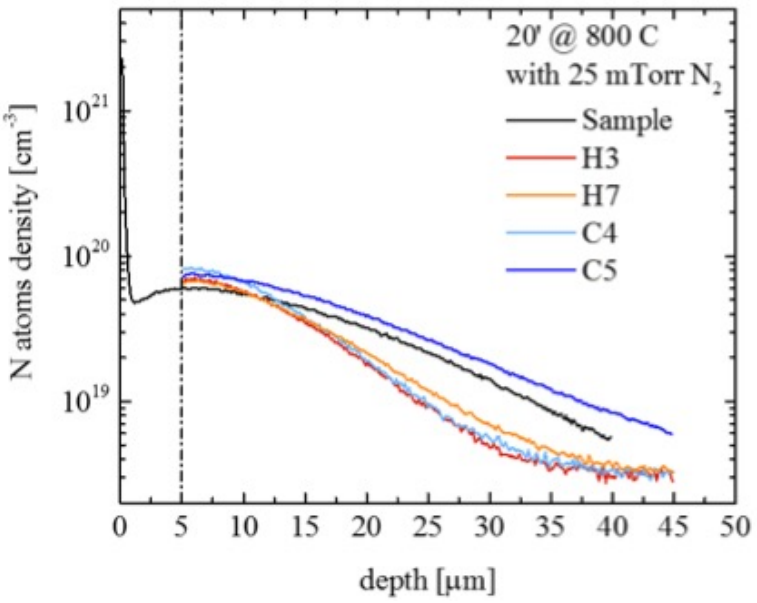

Figure 3: Concentration of nitrogen in the cavity before and after 5 µm of EP. The black curve shows the concentration of NbN on a sample after the doping treatment and before the EP. The other curves show the change in concentration after 5 µm EP, when the nitrides on the surface are removed and only the interstitial nitrogen remains.

4 Measurements

We tested two single cell cavities both with 1.3 GHz resonance frequency and treated with the "2/6" doping recipe, plus 5 µm EP. One cavity was made with Ningxia niobium, the other with Tokyo Denkai. A single cell, 1.3 GHz Nb cavity is shown in figure (4).

We used the Vertical Test Facility at Fermilab to test the radio frequency parameters of the cavities at cryogenic temperature: 1.5 K and 2 K. We equipped the cavities with a temperature mapping system which allows us to know the variation of temperature on the cavity surface. A fast thermometer system has been used on one of the cavities to register the variation of temperature during an interval of time. Both the T-mapping systems were used in order to localize the quench spot of the cavity.

After the RF tests we studied both cavities with optical inspection. We observed the inner surface of the cavities, focusing on the quench region in order to understand if there were asperities, like bumps or holes, in that area.

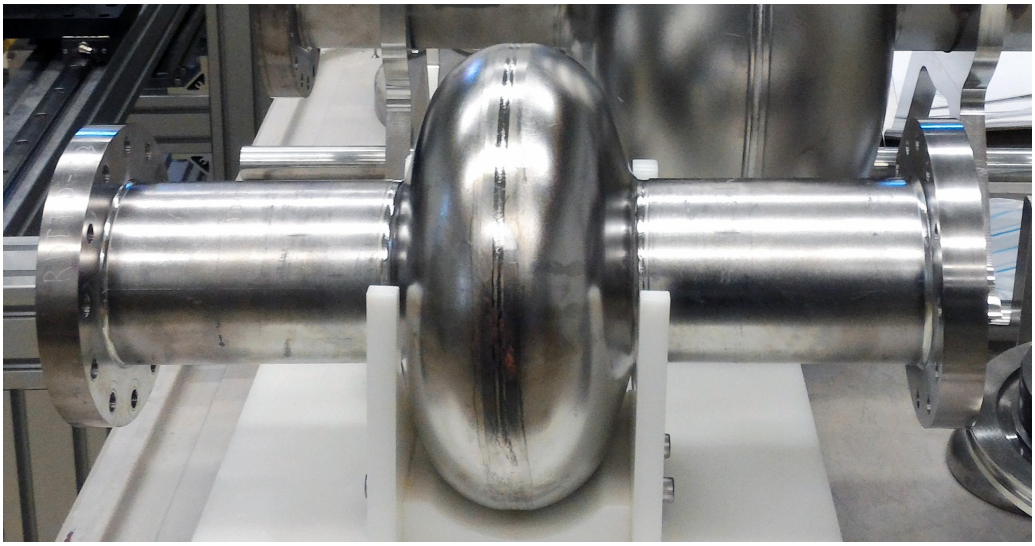

Figure 4: Single cell cavity made of niobium, the resonance frequency is 1.3 GHz.

The following step was the study of cavities' replicas with an optical microscope. We wanted to use laser confocal microscopy to study replicas of the inner surface of the cavities' quench region. Unfortunately we did not have the time to complete this study.

Concerning the niobium samples, we studied the surface using a SEM (scanning electron microscope). We analyzed the samples after the "2/6" treatment, both before and after 5 µm EP. The goal of SEM analyses was to understand if Ningxia and Tokyo Denkai samples show different reaction to the doping treatment.

4.1 RF tests

To reach the cryogenic temperature necessary for the tests, we used one of the pits of the Vertical test facility. The cavity was installed in the pit and helium was poured in the pit in order to completely submerge the cavity with the helium bath.

Before the RF tests, it is important to measure f_0, the exact resonance frequency of the cavity, which depends on the temperature.
For RF tests it is necessary to know f_0 because we use a PLL (phase locked loop) to keep the cavity locked in resonance with the generator. The measurement system is shown in figure (5). A phase locked loop is used to send a RF signal matched with the resonance frequency of the cavity, in order to maximize the amount of power transmitted to the cavity. The PLL uses a feedback system to change the frequency of the RF signal emitted by the generator in order to follow the shifts of f_0 of the cavity.

The following step is to calibrate all the cables that connect the measurement system to the cavity. In this way we can measure the amount of power lost on the cables.

Once the calibration is completed the RF tests can start. During the RF tests, we tested each cavity at 1.5 K and 2 K and we obtained the quality factor versus accelerating field curve. To obtain the values of Q_0 and E_{acc} we measured the power forwarded to and transmitted by the cavity and we converted it using eq. (1) and (8).

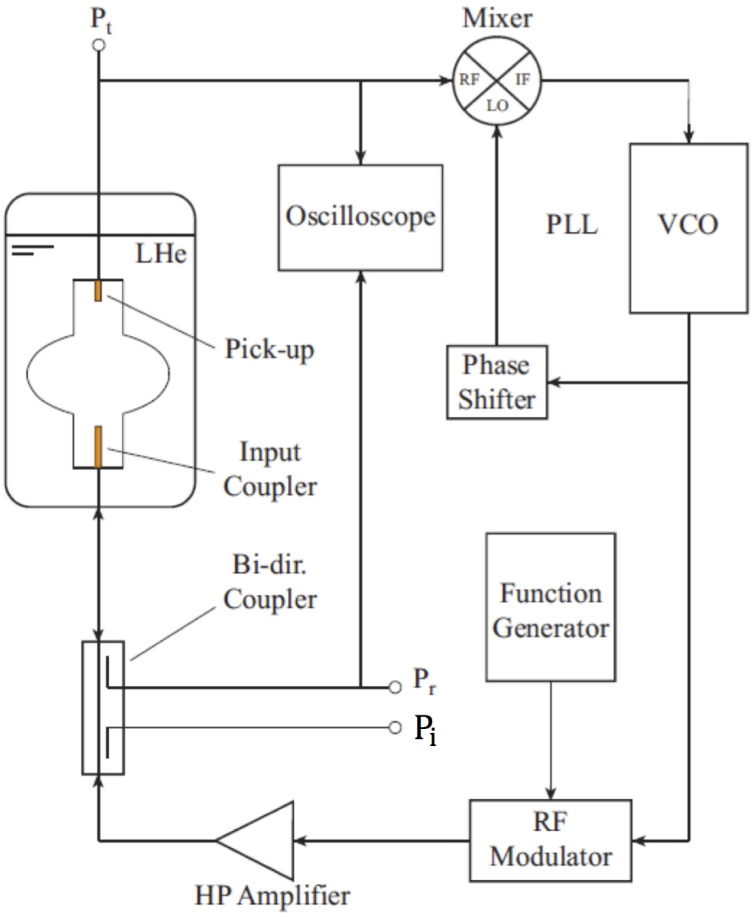

Figure 5: Measurement system of the vertical test.

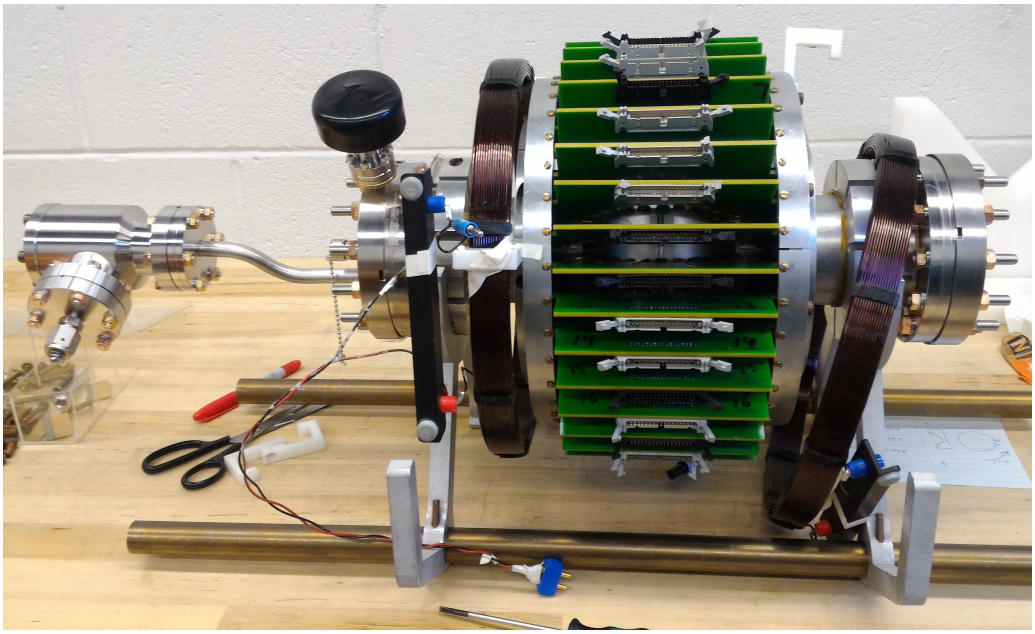

Figure 6: Temperature mapping system: 36 green boards are placed around the cavity, each boards has 16 thermometers which acquire the difference in temperature between the cavity and the helium bath.

4.1.1 Power Rise

We measured the first power rise at 2 K: we started from low values of accelerating field and we gradually increased it. At this temperature we usually don't want the cavity to quench. During a quench the cavity becomes normalconductive and the quench region can trap magnetic flux, which increases the residual resistance R_{res} lowering the quality factor. In order to restore the original, intrinsic quality factor of the cavity it is necessary to warm the cavity, overpassing the critical temperature T_c of the niobium, and then cool it down again to cryogenic temperature. For this reason we usually avoid quench at 2 K in order to be able to continue the measure at 1.5 K.
At 1.5 K we performed a second power rise, starting from low values of E_{acc} and increasing it until the cavity quenched.

4.1.2 T-map system

T-map system is shown in figure (6). The temperature mapping system consists of 36 board, each equipped with 16 thermometers. The boards are placed around the cell, one board every 10°. The cavity equator corresponds to thermometer number 8, while thermometer numbers 1 and 15 shows the temperature at the two irises and thermometer number 16 is placed on the tube beam. The thermometers are resistors, whose resistance varies as a function of the temperature. It is necessary to calibrate the resistors during the cool down of the cavity in order to obtain a thorough measure of ΔT between a point of the cavity and the helium bath.

We used the T-map system to locate the point of quench. We acquired T-maps during the entire power rise in order to understand how a "normal" T-map of that specific cavity appears. This is also useful to understand if the cavity shows heating prior to the quench. Once we reached the quench field and the cavity quenches, we changed the parameters of the forward

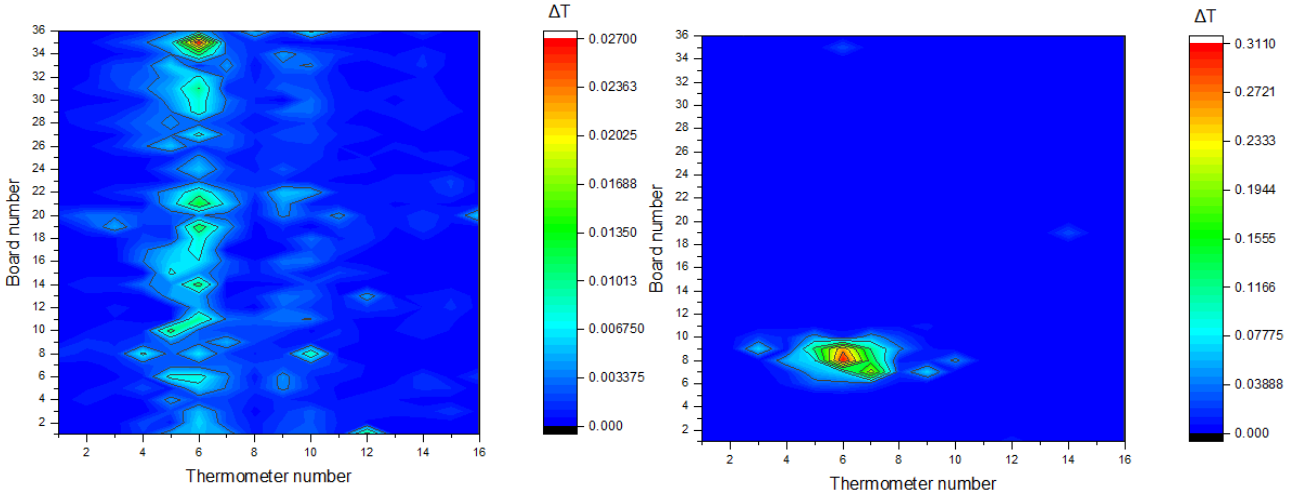

(a) (b)

Figure 7: Figure (a) shows a T-map acquired before the quench event, no heating is found in the spot where the quench will start. The T-map shows two lines of heating at the sides of the equator, where the magnetic field is higher. Figure (b) shows an example of T-map acquired during a quench event. We can see the heating starting from a point and spreading to the surrounding region.

signal in order to quench the cavity continuously. At this point we acquired multiple T-maps in order to capture the quench event. The T-map system allows us to measure the heating that starts from the quench point and spreads to the nearby region. An example of T-map during the power rise and of T-map associated to a quench event is shown in figure (7).

4.1.3 Fast thermometer analysis

During the RF tests of one cavity we used the fast thermometer analysis to track the evolution of the quench. The fast thermometer system uses the same boards and resistors as the T-mapping system, but a different software.
We used t-mapping system to localize the quench area and the resistors connected to that region. We switched to fast thermometer analysis to measure the change in temperature of that set of resistors during an interval of time. We chose Δt so that it would include more than one quench, in order to be sure to register at least one complete event.

4.2 Optical inspection

Once the RF tests were completed and we had analyzed the data to locate all the possible quench spots, we proceeded with the optical inspection of the inner surface of the cavity. We inspected the inner surface of the cavity studying the region of quench and photographed the surface of all the possibile quench spots and other relevant spots where we found asperities. We also studied the rest of the cavity in order to have a comparison.

Figure (8) shows the system we used for the optical inspection. The cavity is installed on a structure which allows to shift the cavity backwards and forwards and also to rotate it. The

camera used for the inspection is installed on the extremity of the black pole and is not visible in the photo because it is already inside the cavity. A laser is installed outside the cavity, in front of the camera, in order to know where the camera is looking. On the two sides of the camera there is a set of lights which can be individually controlled to reach the best lighting. The camera can't shift or rotate, but it can be tilted in order to reach regions far away from the equator.

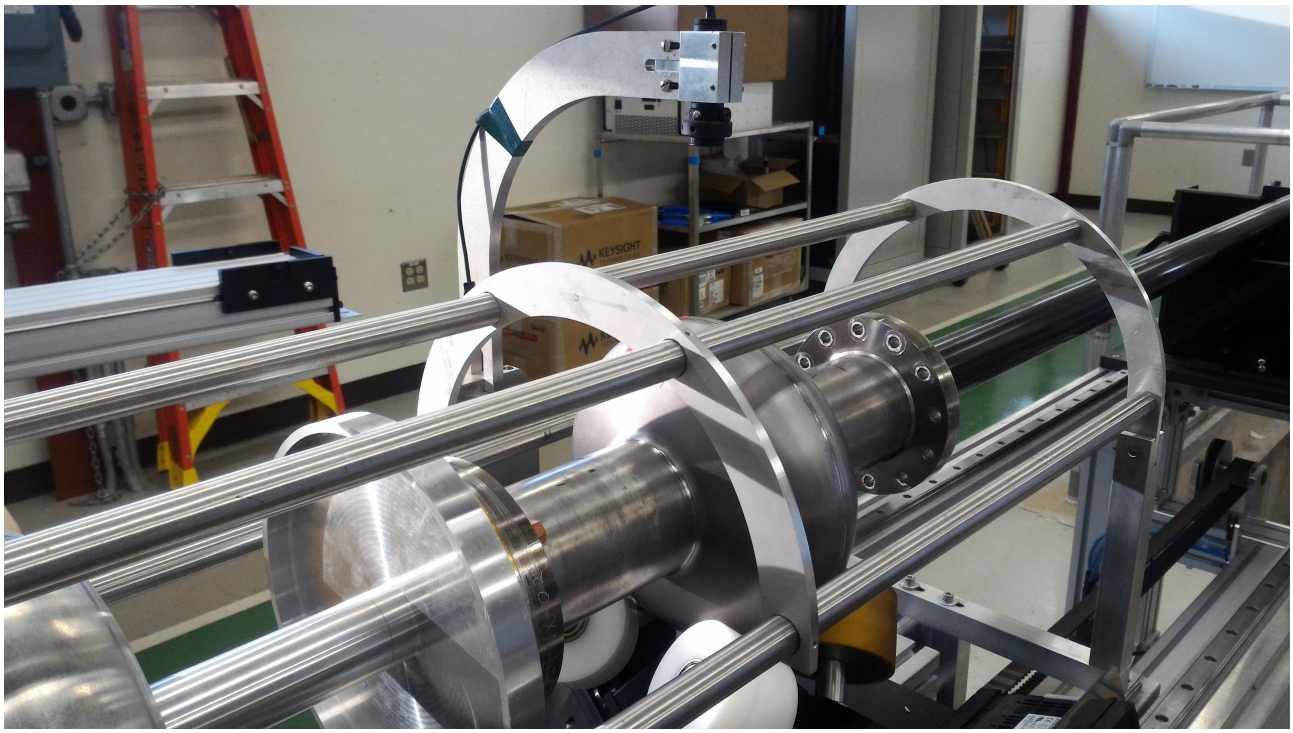

Figure 8: System used for the optical inspection.

4.3 Confocal Laser Scanning Microscopy

With the optical inspection, we identified all the interesting spots of the cavity and we had replicas made from the inner surface of those points. An example of replica is shown in figure (9).

We used the confocal laser microscopy to analyze replicas. Confocal laser scanning microscopy is a technique that allows to combine images of the sample acquired at different depth creating a 3D image. What we wanted to achieve using this technique was to measure the depth of the defects we had found on the surface of the cavity, through the optical inspection.

As already said, we did not had the time to complete this study, we only studied replicas from the quench region of the Ningxia cavity.

4.4 SEM analyses

We used a scanning electron microscope to study the surface of square samples made from Ningxia and Tokyo Denkai niobium. The samples had been treated with "2/6" nitrogen doping

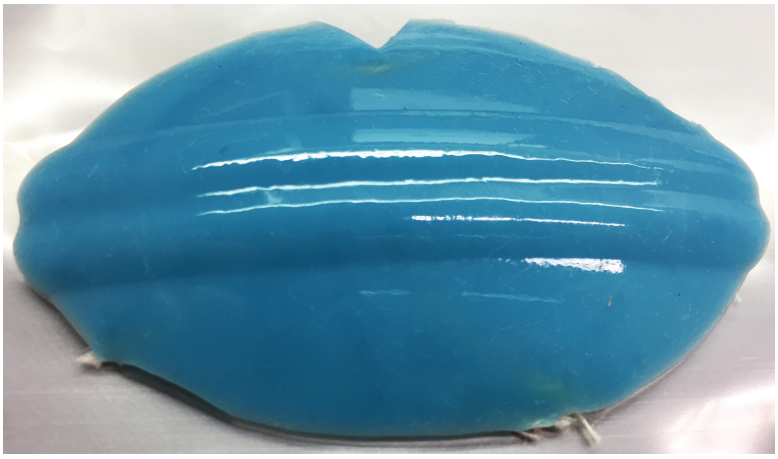

Figure 9: Example of replica of the inner surface of the Ningxia cavity.

and we studied them both before and after 5 µm EP.
We took images of various regions of the samples, and for each region we started from low magnification value (100 µm) to high magnification ($1 \div 2$ µm).
Figure (10) shows multiple samples placed on the stage, ready to be studied with SEM.

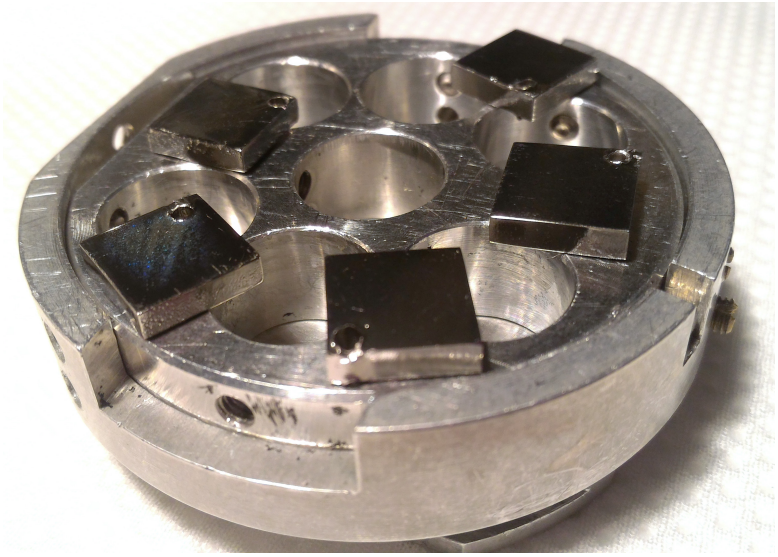

Figure 10: Ningxia and Tokyo Denkai samples placed on the SEM stage.

5 Results

5.1 RF tests

In the next paragraphs are explained the results of the RF tests of the two cavities: the Ningxia cavity (RDTNX002) and the Tokyo Denkai cavity (TE1AES024).

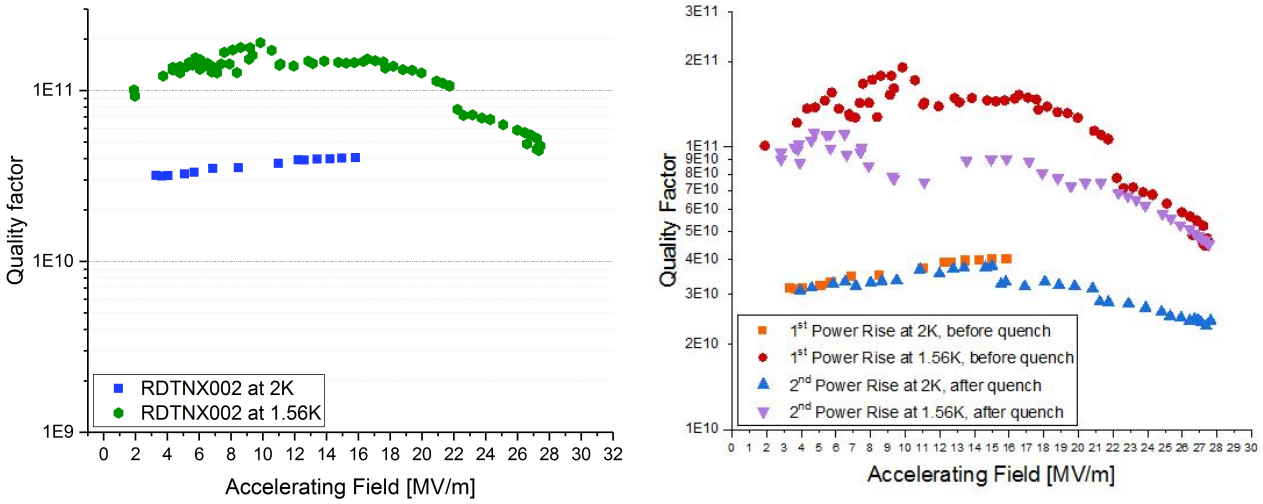

(a) (b)

Figure 11: Figure (a) shows the quality factor versus accelerating field measured at 2 K and 1.5 K during the first power rises. Figure (b) shows a comparison between the quality factor versus accelerating field measured during the first and second set of power rises. In the second sets of measurement, we can see that the cavity shows a lower quality factor. This decrease is due to the trapped magnetic flux that happened during the previous measurements that caused an increase of R_s, affecting the quality factor.

5.1.1 Power Rise

RDTNX002

The results of the first power rise at 2 K and 1.5 K are plotted in figure (11a). During the very first power rise at 2 K we decided not to quench the cavity in order to avoid magnetic flux trapping and for this reason we stopped the power rise at 16 MV/m.
At 1.5 K we performed the whole power rise until the cavity quenched at $E_{acc}(quench) = 27.3\,\mathrm{MV/m}$.

After the first set of power rises, it wasn't possibile to warm the cavity above T_c and cool it back down to 2 K. For this reason the following power rises we measured present a lower quality factor due to the magnetic flux trapped in the quench region. The result of these two power rises is shown in figure (11b). The increase of R_s caused by the trapped magnetic flux is analyzed in the following section.

TE1AES024

For the Tokyo Denkai cavity we measured a first power rise at 2 K, reaching the quench at $E_{acc}(quench) = 20\,\mathrm{MV/m}$.

Before measuring the following power rise at 1.5 K, we increased the temperature of the helium bath above the critical temperature of the niobium, $T_c = 9.25\,\mathrm{K}$, and then we cooled it down again. In this way we eliminated the magnetic flux trapped into the quench region, restoring the intrinsic value of the quality factor. Once we reached $T = 1.5\,\mathrm{K}$, we measured a second power rise. The results of both power rises are plotted in figure (12).

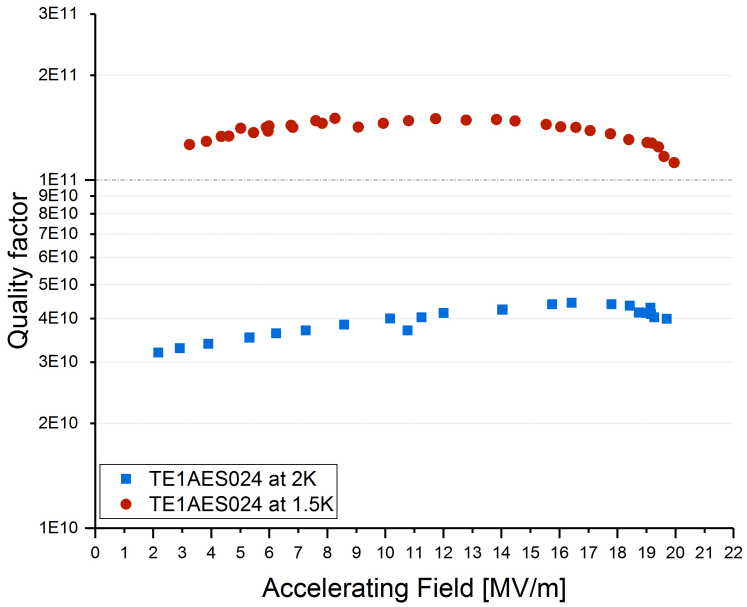

Figure 12: Plot of quality factor versus accelerating field measured at 2 K and 1.5 K. At both temperatures the cavity quenched at $E_{acc}(quench) = 20\,\mathrm{MV/m}$

Cavity	Q_0 at 2 K	Q_0 at 1.5 K
RDTNX002	$4 \cdot 10^{10}$	$1.5 \cdot 10^{11}$
TE1AES024	$4.4 \cdot 10^{10}$	$1.4 \cdot 10^{11}$

Table 1: Quality factor measured at 16 MV/m at 2 K and 1.5 K for both cavities.

5.1.2 Surface Resistance

From the measure of quality factor we can also obtain a measure of the surface resistance R_s, using $Q_0 = G/R_s$.

RDTNX002

We used the second set of power rise to decompose R_s into R_{res} and R_{BCS}.
At 1.5 K, we know that the R_{BCS} term is negligible, so we have $R_s = R_{res}$, and
$R_{res} = R_0 + R_{flux}$.
We had measured, for fixed values of the accelerating field, how the quality factor changed with temperature between 2 K and 1.5 K in order to obtain R_{res}. We fitted the values of R_{res} to extract R_0, and then we interpolated R_{res}. We used the measurement at 2 K to extract $R_{BCS} = R_s - R_{res}(interpolated)$.

The result of the decomposition of R_s into R_{res} and R_{BCS} is shown in figure (13). As expected from the nitrogen doping, R_{BCS} shows a decrease for medium values of the accelerating field.

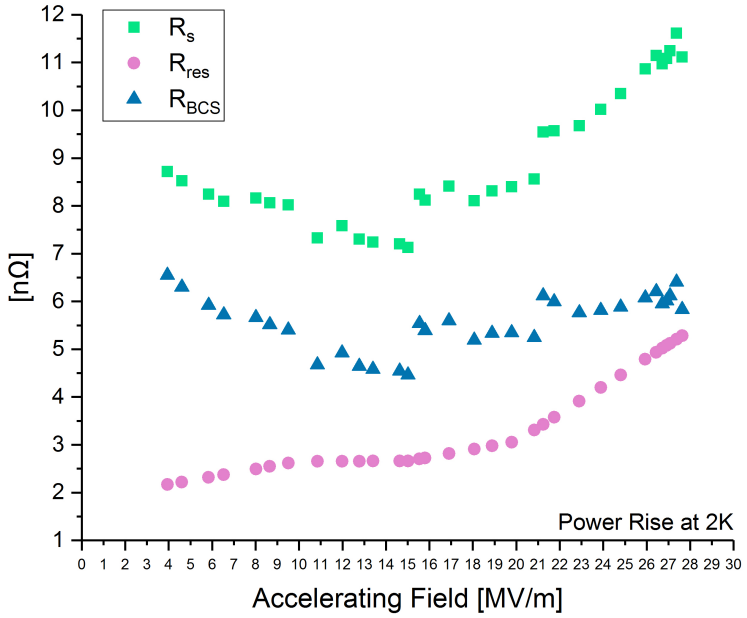

Figure 13: RDTNX002: Plot of R_s decomposed into R_{res} and R_{BCS}.

TE1AES024

For the Tokyo Denkai cavity, the decomposition of R_s was easier since we had eliminated the term of R_{flux} warming the cavity above T_c and cooling it again before the second power rise. We used the measurement of the quality factor at 1.5 K to extract R_0. Then we subtracted R_0 to R_{res} measured at 2 K to extract R_{BCS}.
The result of the decomposition is shown in figure (14). As for the other cavity, we can see R_{BCS} decreasing for medium values of the accelerating field. We can't see the following increase for higher values of E_{acc} because the cavity quenched at 20 MV/m.

5.1.3 T-map system

We acquired T-maps both during power rises, both during quench events.

RDTNX002

For the Ningxia cavity, during a power rise we noticed that some thermometers were starting to heat up before the quench. Comparing T-maps acquired during the power rise with T-maps associated to quench events, we discovered that the quench started from the same thermometers that showed pre-heating.

In figure (15) is shown the plot of ΔT versus E_{acc}. This data has been acquired during the first complete power rise at 1.5 K.

Figure (16a) shows a quench event photographed by the T-map system. The area that shows heating is where the quench happened. Figure (17) shows another T-map associated to a quench, here only a few point of the quench area are highlighted. This can help us understand the specific points from which the quench starts.
In this cavity the quench region appears to be on the equator, where the magnetic field is not

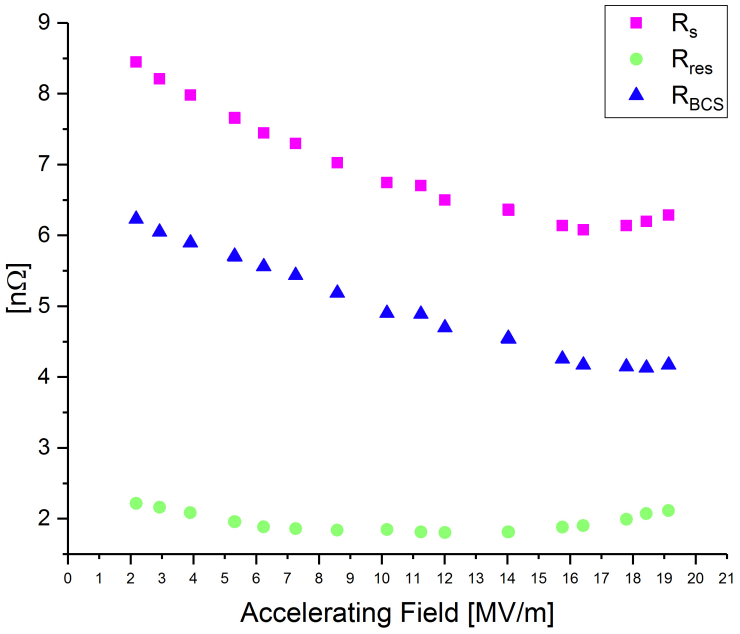

Figure 14: TE1AES024: Plot of R_s decomposed into R_{res} and R_{BCS}.

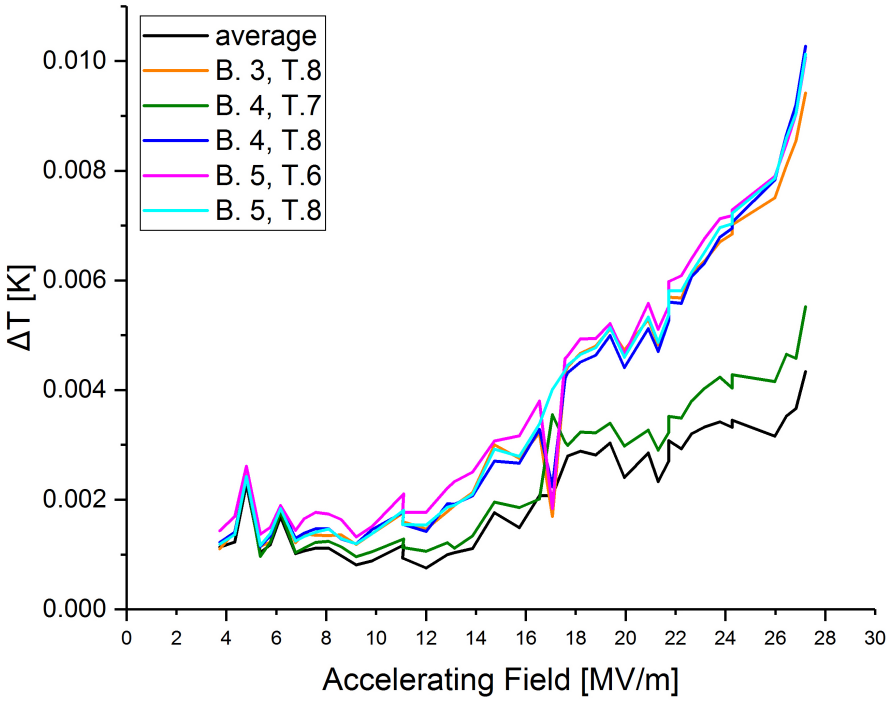

Figure 15: RDTNX002: Plot of ΔT versus E_{acc}, measured during the first power rise at 2 K. The thermometers involved in the quench show pre-heating starting from the first power rise. The average value of ΔT of the T-map is plotted for comparison.

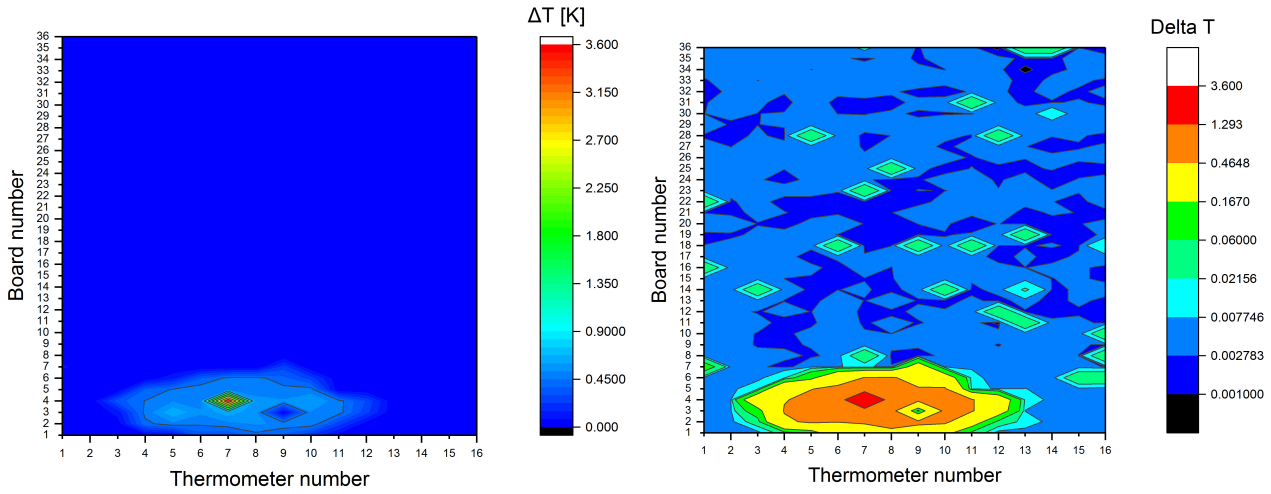

(a) (b)

Figure 16: RDTNX002: Figure (a) shows a temperature map of a quench event at 2 K. The quench region is spreading on boards 3,4,5, thermometers 4 to 11. Figure (b) shows the same T-map plotted in logarithmic scale to highlight the quench area.

maximum.
The quench region location and the fact that the cavity shows pre-heating suggests that the quench is not magnetic induced, but is caused by thermal breakdown. This means that the point where the quench will happen starts heating and dissipating, spreading heat to the neighbouring region, until the temperature reaches T_c. When $T = T_c$, the area becomes normalconductive and the cavity quenches.

TE1AES024

Studying the temperature maps acquired during quench events, we understood that the quench area was far from the equator, as can bee seen from figure (19), where the magnetic field is higher.

For the Tokyo Denkai cavity, we found that the cavity did not present any heating prior to the quench. The plot of ΔT versus E_{acc} is shown in figure (20).

5.1.4 Fast thermometer analysis

TE1AES024

We used T-maps like figure (19) to understand which set of thermometers we had to study with the fast thermometer analysis.
Once identified the correct matrix of thermometers, and eliminated the thermometers that didnt show any heating, we obtained a plot as figure (21). Comparing fast thermometer analysis' plot to the temperature maps, we conclude that the spots responsible for the quench are located on boards 19, 20, thermometer 12.

The absence of pre-heating during the power rise, and the location of the quench spot where the magnetic field is maximum makes us believe that the quench has magnetic nature.

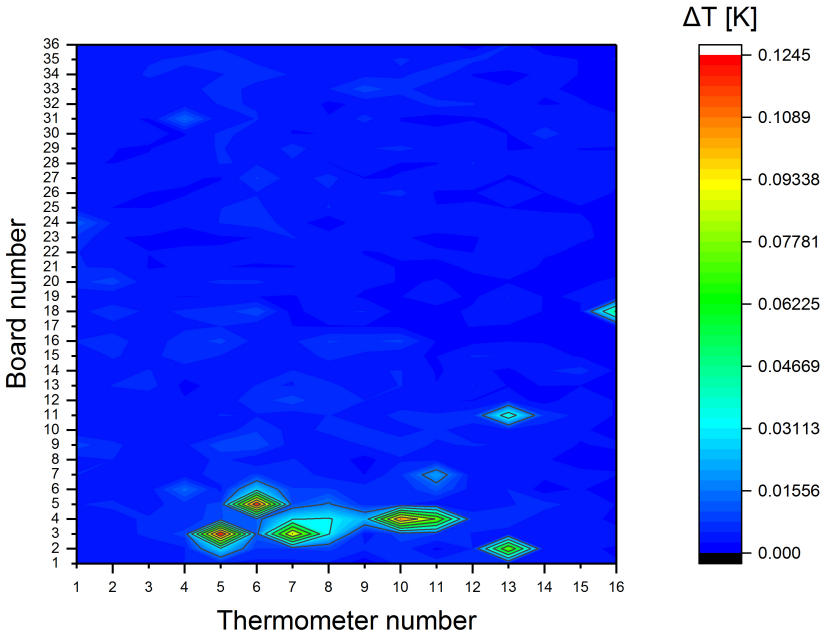

Figure 17: RDTNX002: Temperature map of a quench event. Here not the entire quench area is heated, we can distinguish a few points belonging to the quench area.

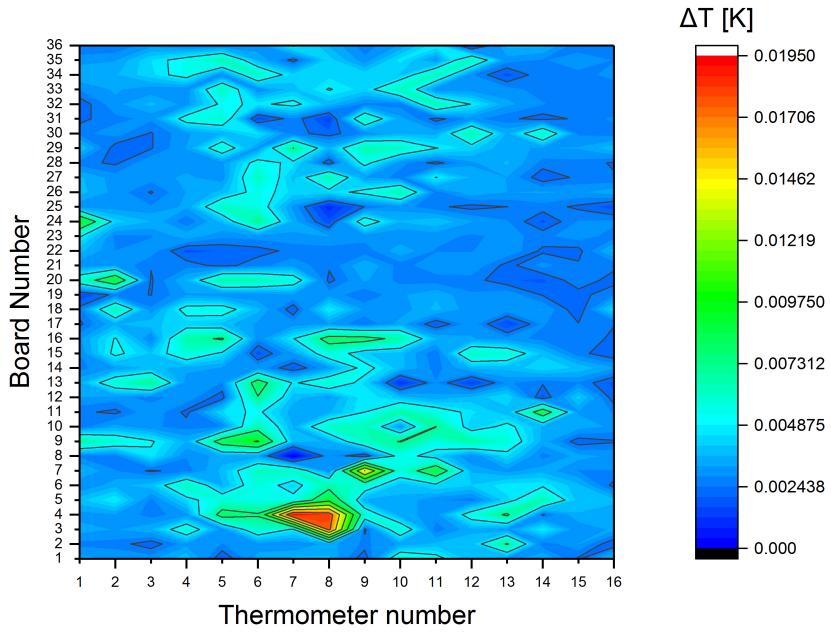

Figure 18: RDTNX002: Temperature map acquired during the second power rise at 2 K. Due to the magnetic flux trapped into the quench area during previous measurements, we can see that the quench spot is heated before the quench.

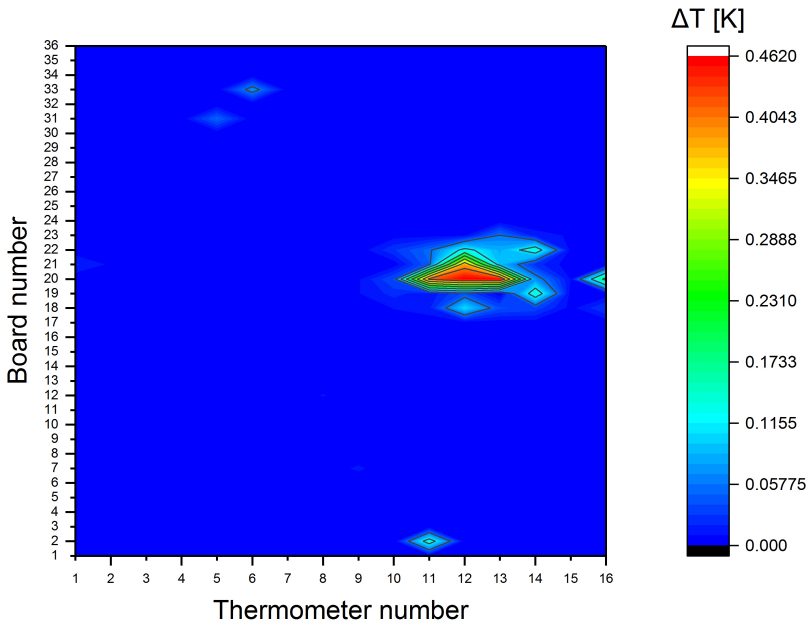

Figure 19: TE1AES024: temperature map of a quench event at 2 K. The quench region is spreading on boards 19 to 22, thermometers 10 to 14.

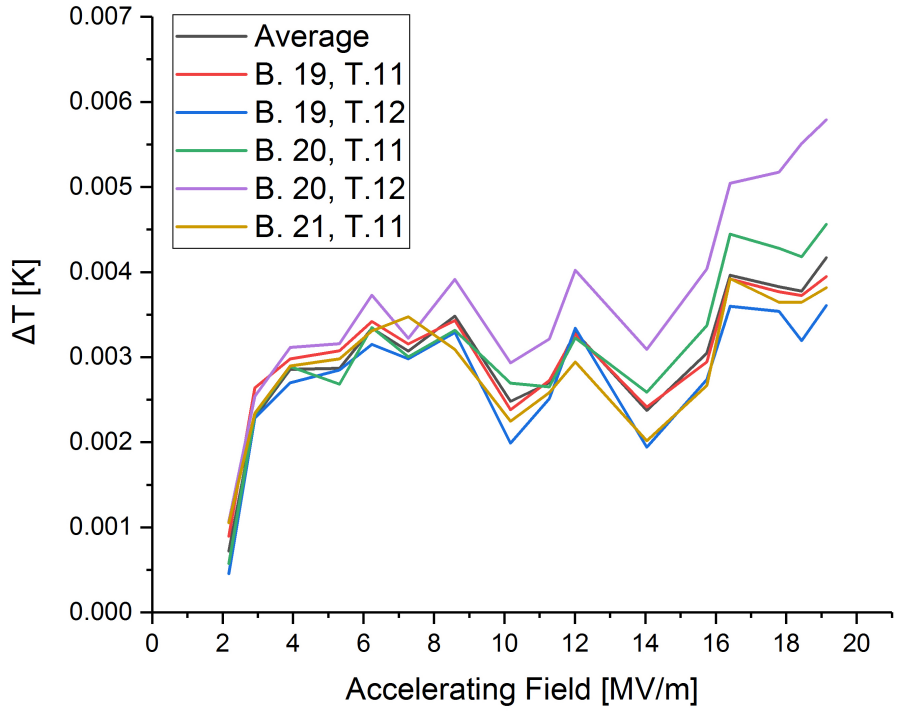

Figure 20: TE1AES024: Plot of ΔT versus E_{acc}, measured during the first power rise at 2 K. The thermometers involved in the quench don't show any heating prior to quench. The average value of ΔT of the T-map is plotted for comparison.

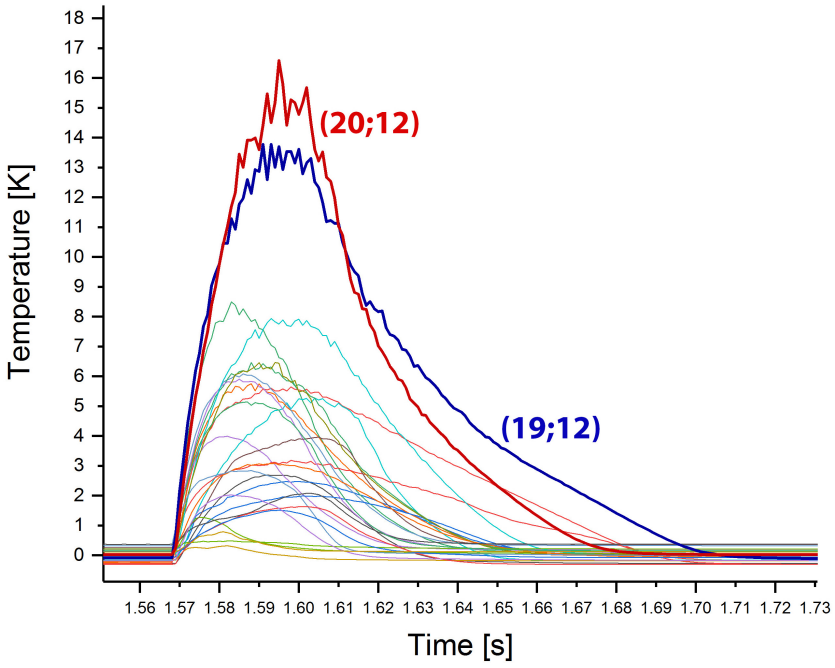

Figure 21: TE1AES024: T vs time, measured for a matrix of thermometers including the quench area. We have highlighted the thermometers that reach the highest temperatures and that we believe are the starting point of the quench.

5.2 Optical inspection

We analyzed the surface on the quench spot and we compared it to the surface of the whole cavity.

RDTNX002

For the Ningxia cavity we noticed that the welding on the equator presented various irregularities, both bumps and holes. These morphological defects were located both in and out of the quench region. From the optical inspection we are not able to determine the depth of the defects.
Figures (22), (23), (24) show some examples of defects we found on the surface.

For comparison, figure (25) shows some examples of areas of the surface that don't show any defects or pronounced grain boundaries.

TE1AES024

For the Tokyo Denkai cavity we didn't find any morphological defects on the surface. However, we noticed that the surface showed pronounced steps at the grain boundaries, as can be seen from figures (26) and (27).

Figure (28) shows a region of the equator of the cavity, the welding looks different from cavity RDTNX002's equator (fig: (22c), (25a)).

For the cavity TE1AES024, we think that the quench has magnetic nature and that the pronounced steps at the grain boundaries cause an enhancement of the local magnetic field, such that it overpasses the critical magnetic field, causing the quench.

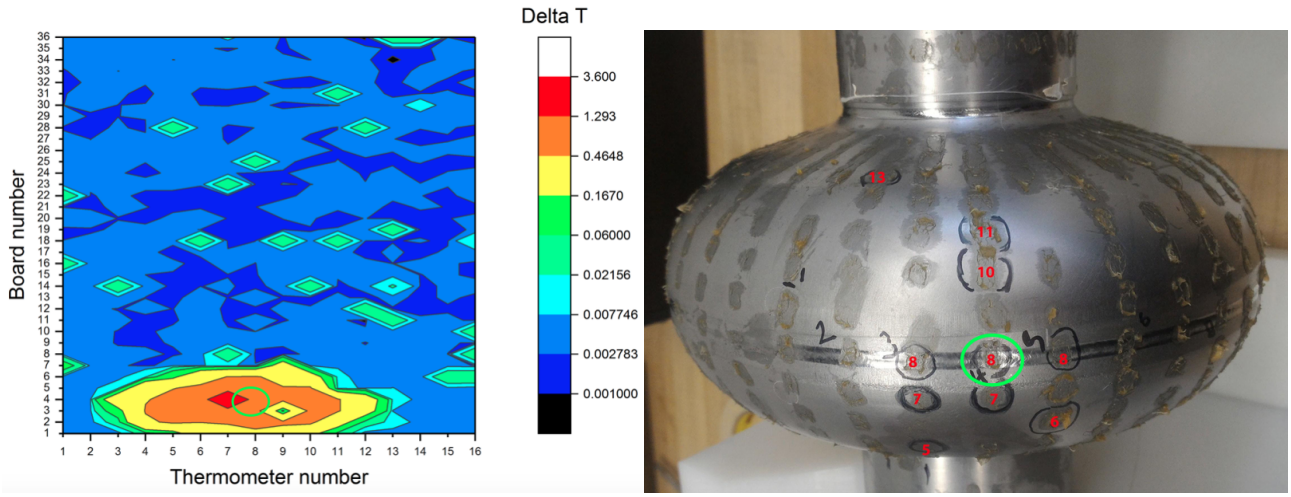

(a) (b)

(c)

Figure 22: RDTNX002: Figure (a) shows a T-map associated to a quench event. Figure (b) shows the outer surface of the cavity, once the T-map boards have been removed. On the cavity a trace of the resistors remains; we used these traces to identify the quench region. Both on figure (a) and (b) we have highlighted the point shown on figure (c): board 4, thermometer 8. In figure (c) the inner surface of point (4; 8) is shown. On the right side of the welding a hole in the surface is visible.

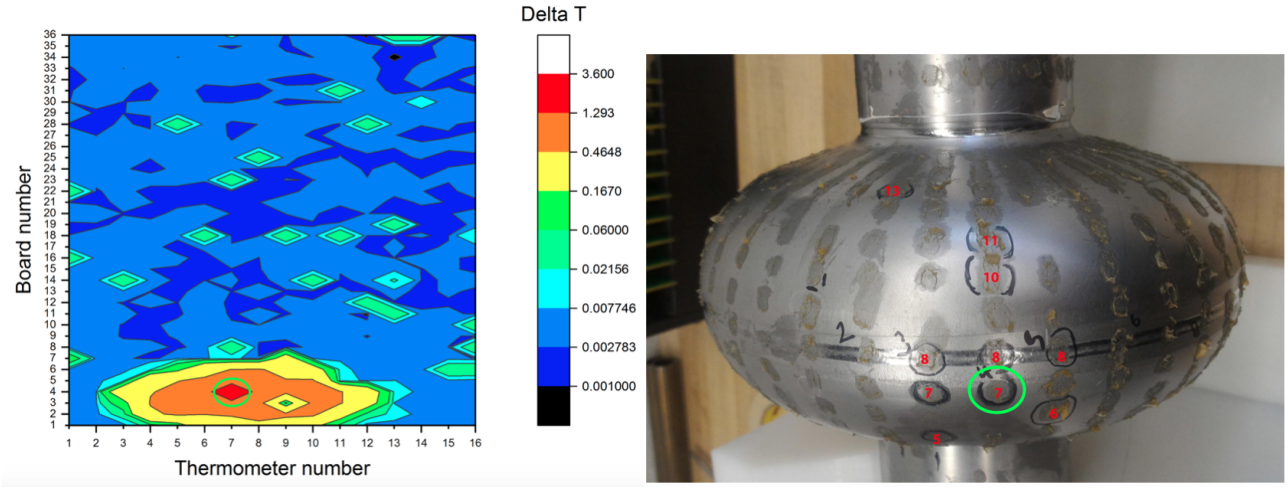

(a) (b)

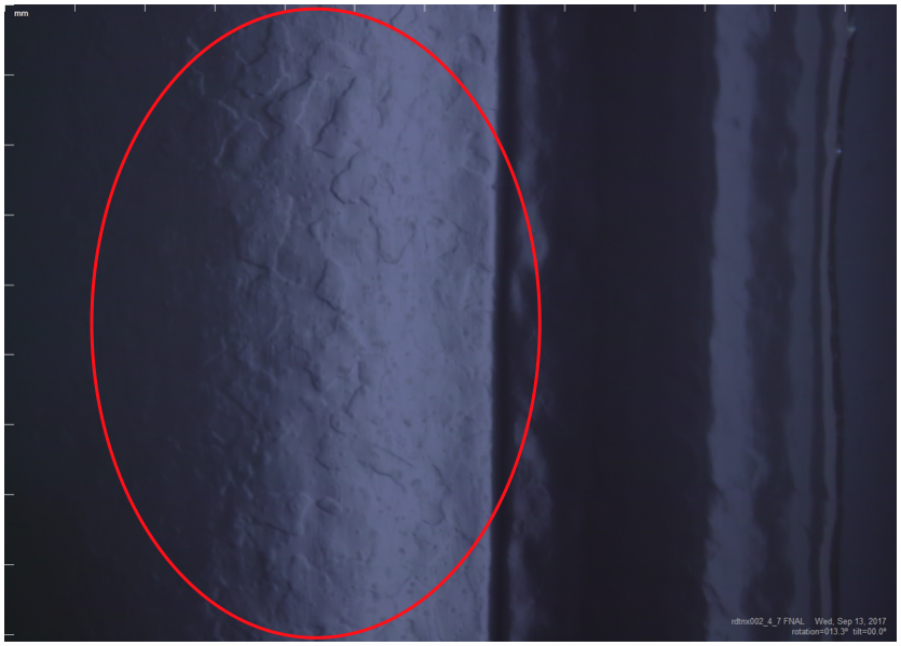

(c)

Figure 23: RDTNX002: Figure (a) shows a T-map associated to a quench event. Figure (b) shows the outer surface of the cavity, once the T-map boards have been removed. On the cavity a trace of the resistors remains; we used these traces to identify the quench region. Both on figure (a) and (b) we have highlighted the point shown on figure (c): board 4, thermometer 7. In figure (c) is shown the inner surface of point (4; 7). Here we can see no important defect but the grain boundaries are clearly visible.

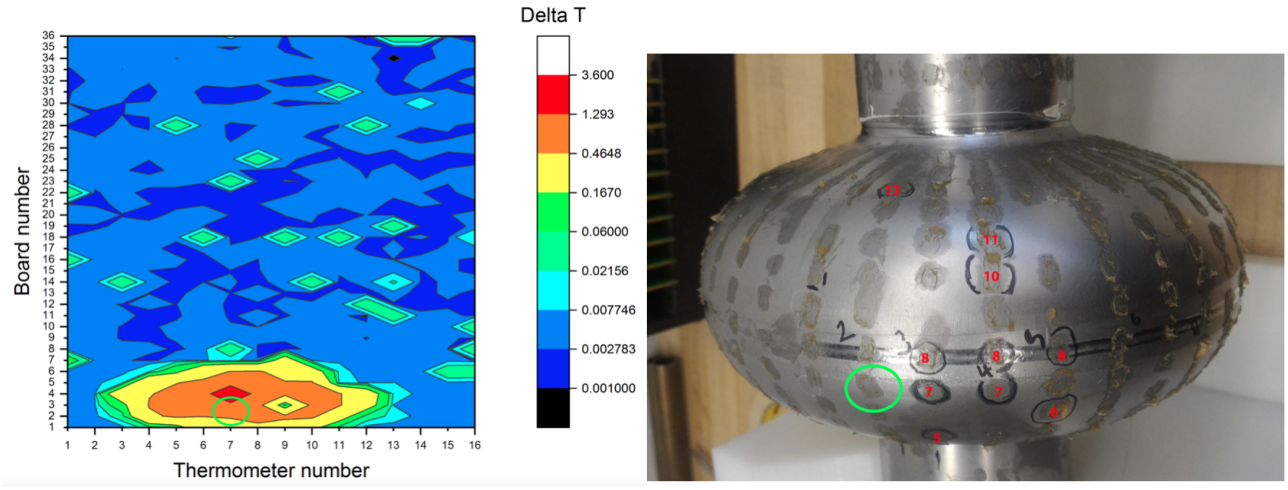

(a) (b)

(c)

Figure 24: RDTNX002: Figure (a) shows a T-map associated to a quench event. Figure (b) shows the outer surface of the cavity, once the T-map boards have been removed. On the cavity a trace of the resistors remains; we used these traces to identify the quench region. Both on figure (a) and (b) we have highlighted the point shown on figure (c): board 4, thermometer 7. In figure (c) the inner surface of point (2; 7) is shown. We can clearly see a bump on the surface. This point didn't belong to the quench spots.

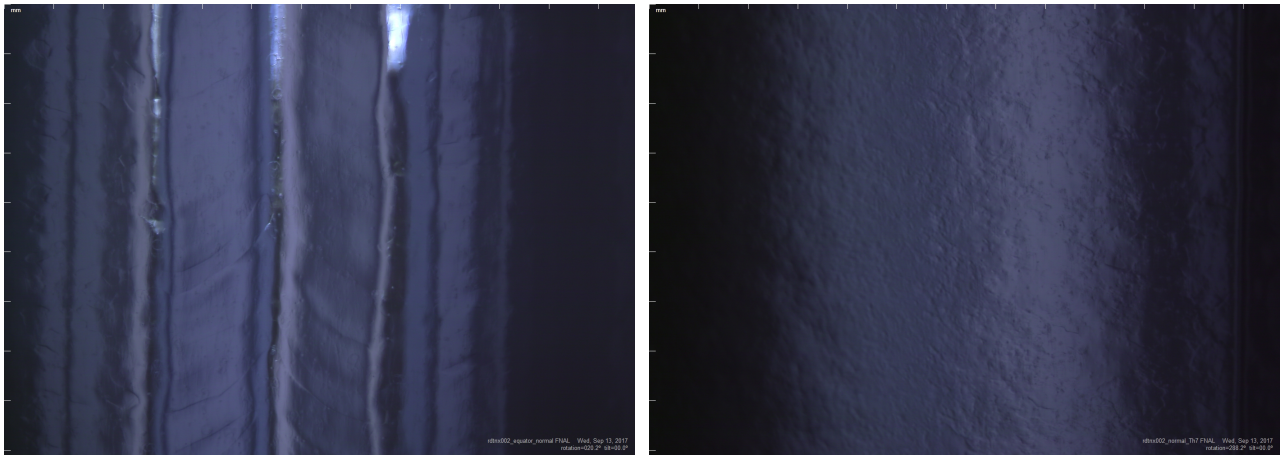

(a) (b)

Figure 25: RDTNX002: Figure (a) shows a point of the equator without specific defects. However even here, the three sides of the welding appear excessively pronounced. For comparison see figure (28). Figure (b) shows an example of surface without pronounced grain boundaries.

5.3 Confocal Laser Scanning Microscopy

We analyzed some replicas of the quench region of the Ningxia cavity.

RDTNX002

From the analysis of replicas of the equator region (boards 3,4,5; thermometer 8), we found a depression involving the center and both sides of the welding. Thanks to the confocal laser microscopy we were able to measure the defect on the replica. On the replicas, we found a bump 10 mm long and at least 150 µm high, it is shown in figure (29). To measure the height of the bump we used the area circled in yellow in figure (29b). Here we noticed a sharp step in the vertical profile of the welding, as shown in figure (29c).
This is coherent with the presence of morphological defects we had noticed from the optical inspection. From this first study of the replicas we didn't find the exact same defects that we had seen with the optical inspection.
Further analyses of the replicas would be necessary.

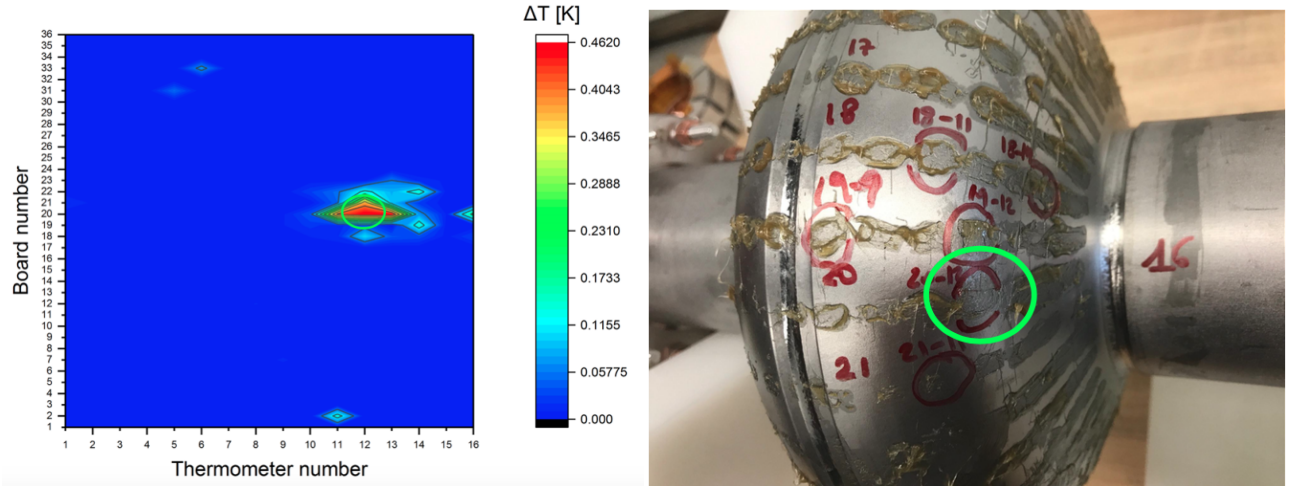

(a)

(b)

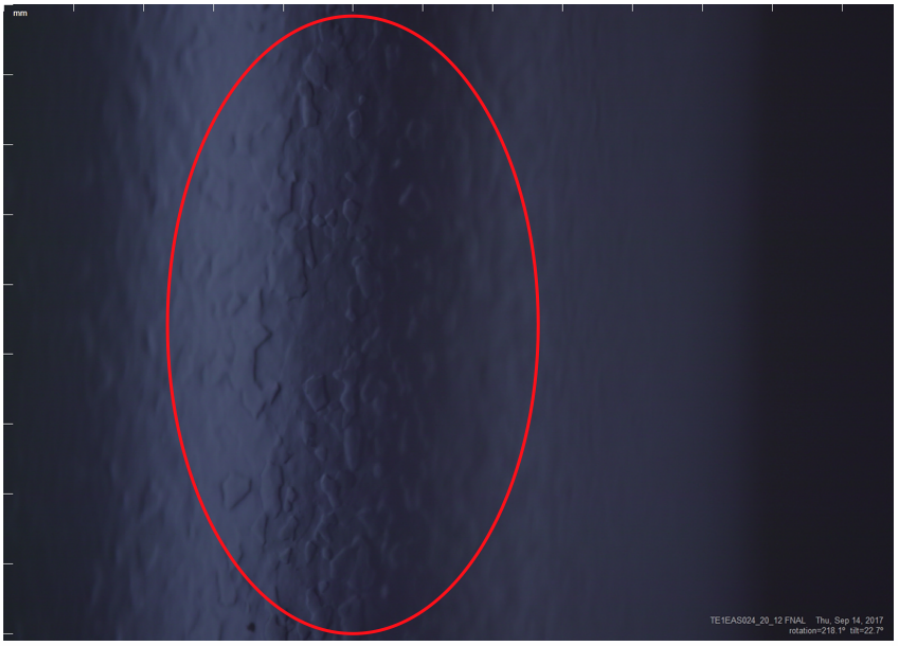

(c)

Figure 26: TE1AES024: Figure (a) shows a T-map associated to a quench event. Figure (b) shows the outer surface of the cavity, once the T-map boards have been removed. On the cavity a trace of the resistors remains, we used these traces to identify the quench region. Both on figure (a) and (b) we have highlighted the point shown on figure (c): board 20, thermometer 12. In figure (c) is shown the inner surface of point (20; 12).

Figure 27: TE1AES024: Another region of the cavity (board 23, thermometer 19) showing pronounced steps at the grain boundaries.

Figure 28: TE1AES024: Region of the equator without defects, the welding looks different from the equator of cavity RDTNX002, more regular and both the center and the sides of the welding are less pronounced.

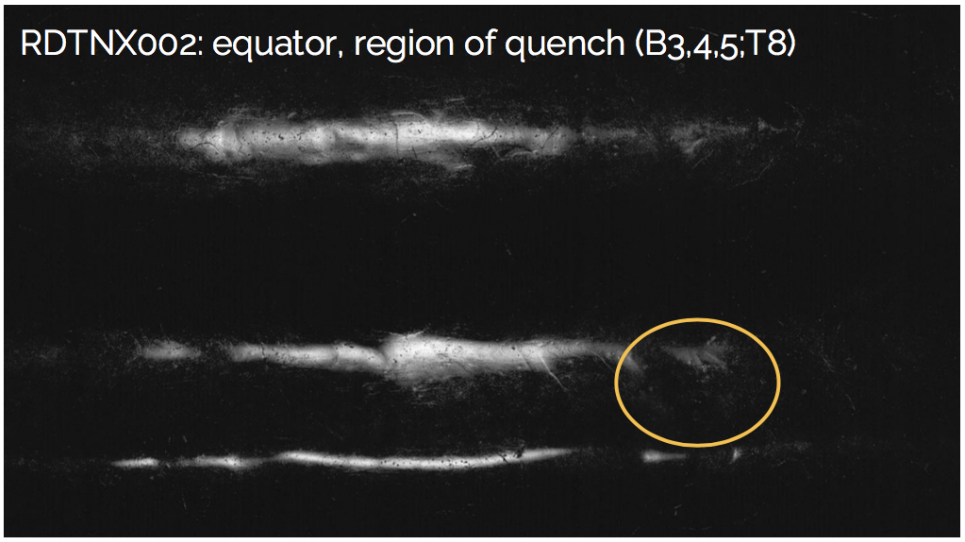

(a)

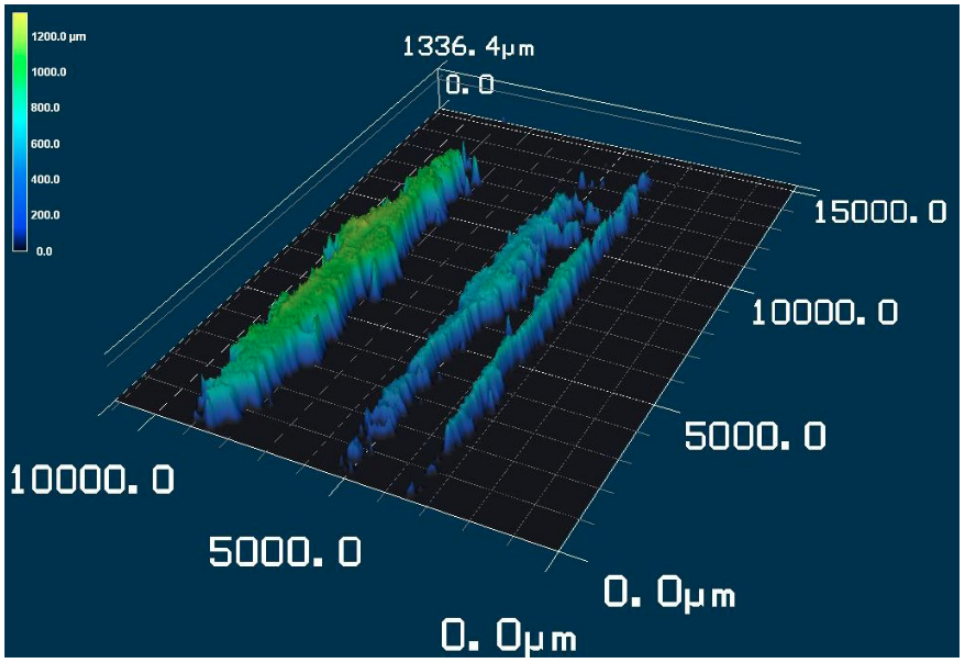

(b)

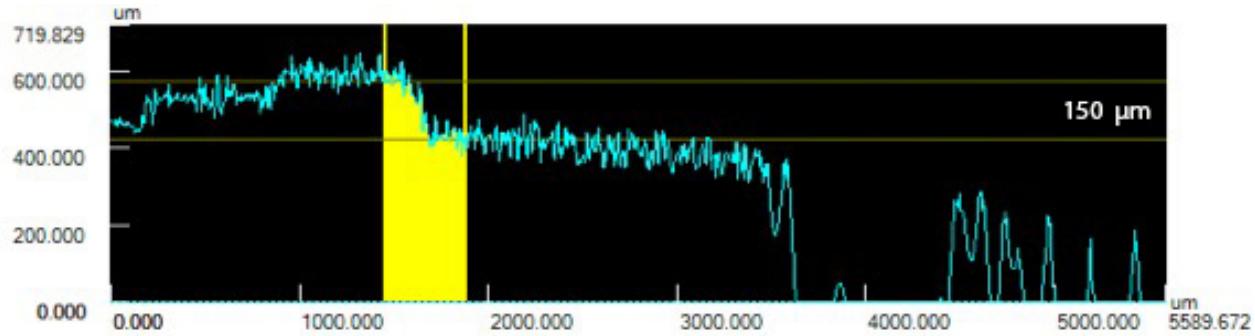

(c)

Figure 29: RDTNX002: Figure (a) shows the center and the two sides of the welding. The area circled in yellow is where we measured the height of the bump. Figure (b) shows the 3D profile of the welding. Figure (c) shows the vertical profile of the center of the welding, the step we measured is highlighted in yellow.

5.4 SEM analyses

We used a scanning electron microscope to study samples of Ningxia and Tokyo Denkai, doped with the "2/6" recipe, before and after 5 µm EP.

Ningxia samples, before EP

As expected from a nitrogen doped sample treated with the "2/6" recipe, on the surface of the Ningxia samples we found "birds" of nitrides. These phases of NbN are visible starting from a magnification corresponding to 10 µm. The highest magnification achievable with our SEM corresponds to 1 µm. Studying different regions of the samples we noticed a different concentration of nitrides in different grains, we could clearly see the change in concentration on the two sides of a grain boundaries. This is shown in figure (30).

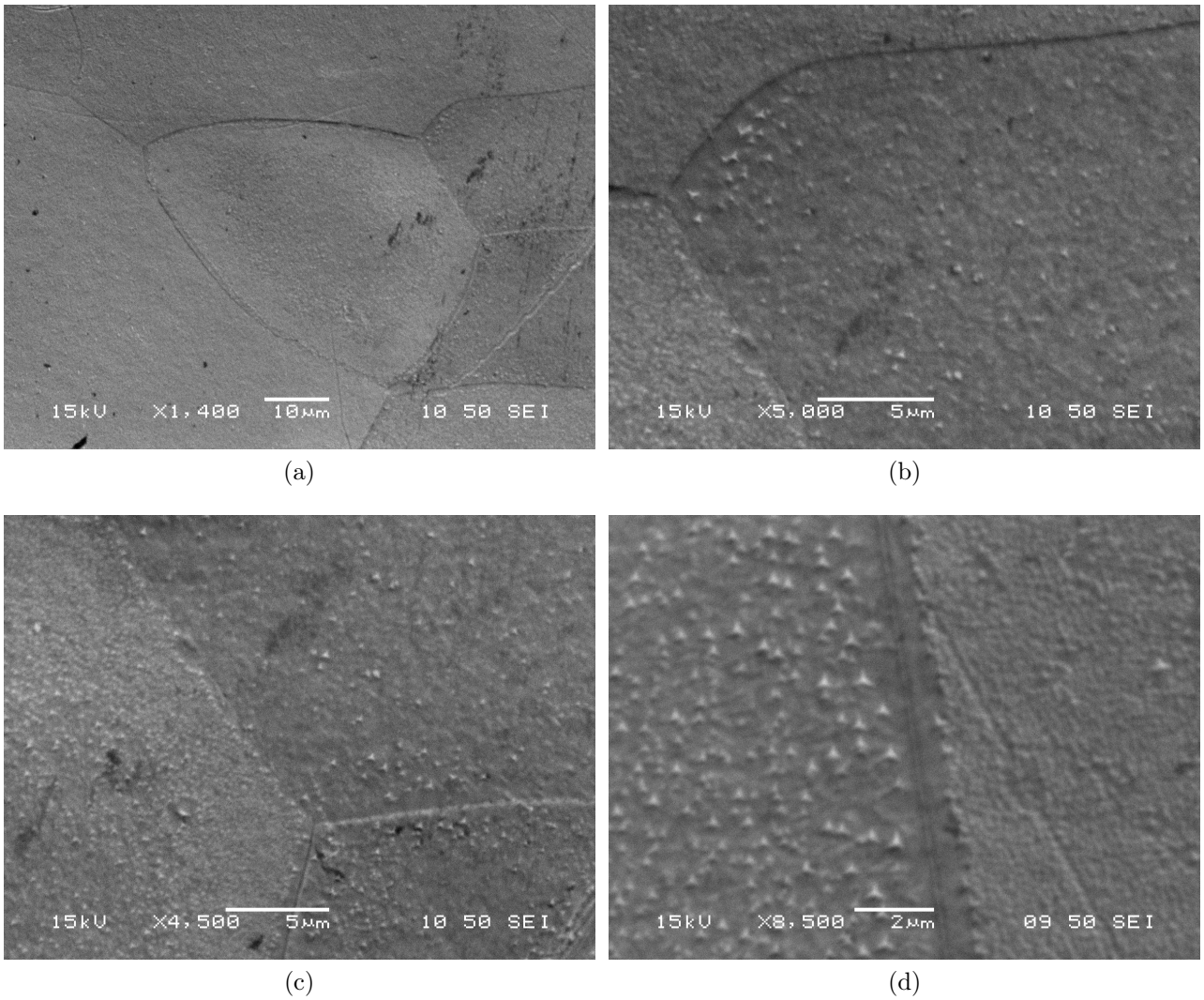

(a) (b)

(c) (d)

Figure 30: Ningxia Samples, before EP: Figure (a) shows different grains of niobium, the nitrides start to be visible on some grains. Figures (b), (c), (d) show nitrides growing with different concentration in different grains. The images show different magnifications and regions of the sample.

Tokyo Denkai samples, before EP

Tokyo Denkai samples showed a completely different pattern on the surface. We didn't find any "birds" of nitrides on the surface. The SEM images of the samples are shown in figures (31), we think that the pattern we found is a different phase of NbN nitrides.
In order to better understand this pattern it is necessary to study Tokyo Denkai samples with different instruments, more appropriate to study the nature of the NbN phase.

As for the Ningxia samples, we noticed that growth of this NbN phase is different in different grains, as can be seen from figures (31a) and (31b). Studying the samples we noticed that Tokyo Denkai showed pronounced steps at the grain boundaries, as shown in figure (31d). This observation is in agreement with what we noticed from the optical inspection.

From SEM study we can conclude that the two materials react differently to the same nitrogen-doping treatment. The causes of this difference are yet to be cleared, and further studies are necessary to understand how this can affect the perfomances of cavities made with Ningxia or Tokyo Denkai niobium.

Ningxia and Tokyo Denkai samples, after 5 µm EP

We decided to analyze a sample of Ningxia and one of Tokyo Denkai also after 5 µm EP.
As expected, all the nitrides have been removed through electropolishing.
We noticed that, despite the EP, the Tokyo Denkai sample still has pronounced steps at the grain boundaries. The comparison between the Ningxia sample and the Tokyo Denkai is shown in figure (32). This observation is in agreement with the results of the optical inspection of the Tokyo Denkai cavity (TE1AES024, figure (27)).

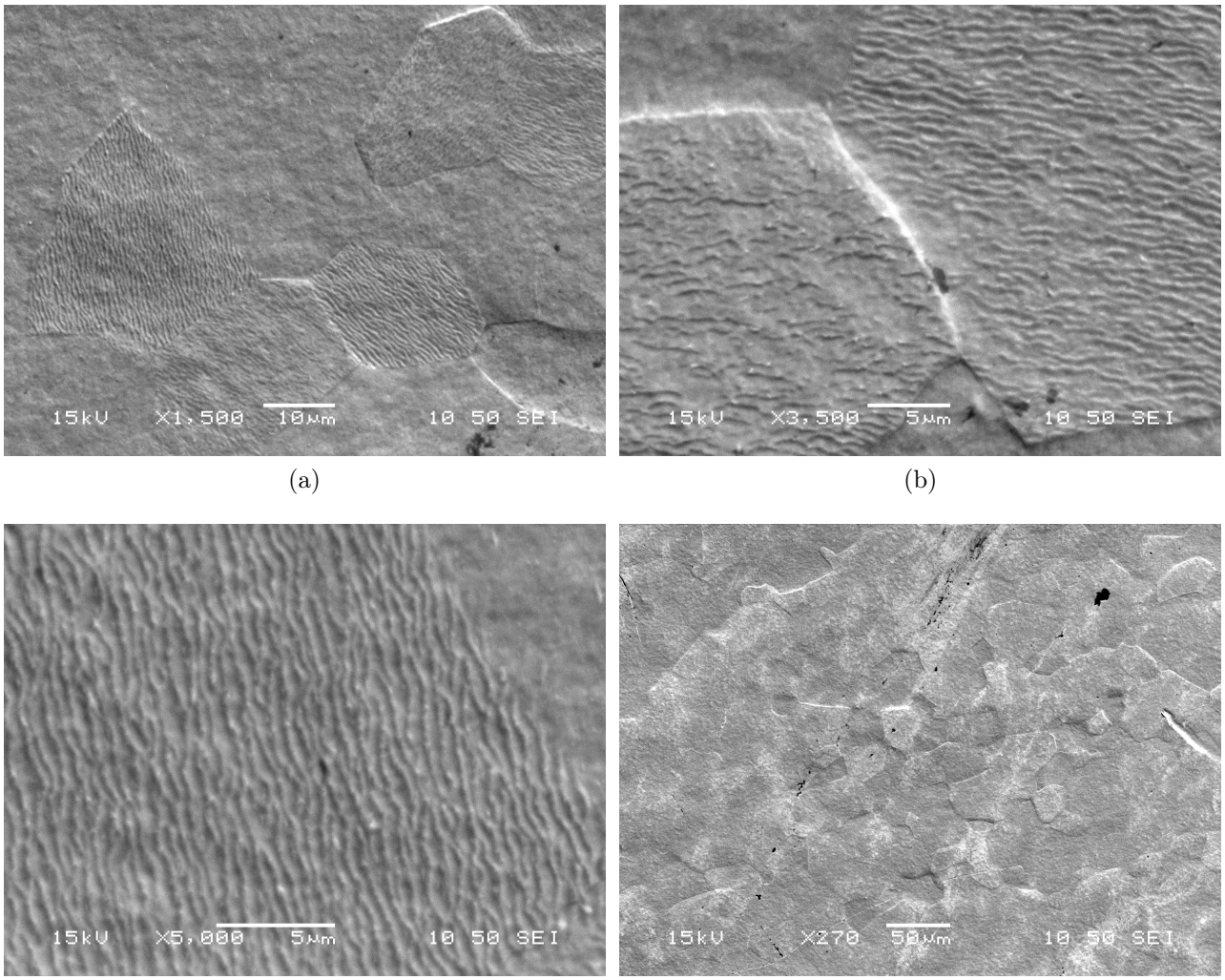

(a) (b)

(c) (d)

Figure 31: Tokyo Denkai Samples, before EP: Figure (a) shows different grains of niobium, NbN phases are visible only in some grains. Figure (b) shows nitrides growing differently in different grains. Figure (c) shows a zoomed image of the NbN pattern. Figure (d) shows a Tokyo Denkai sample with a lower magnification: we can distinguish different grains and notice pronounced steps at the grain boundaries.

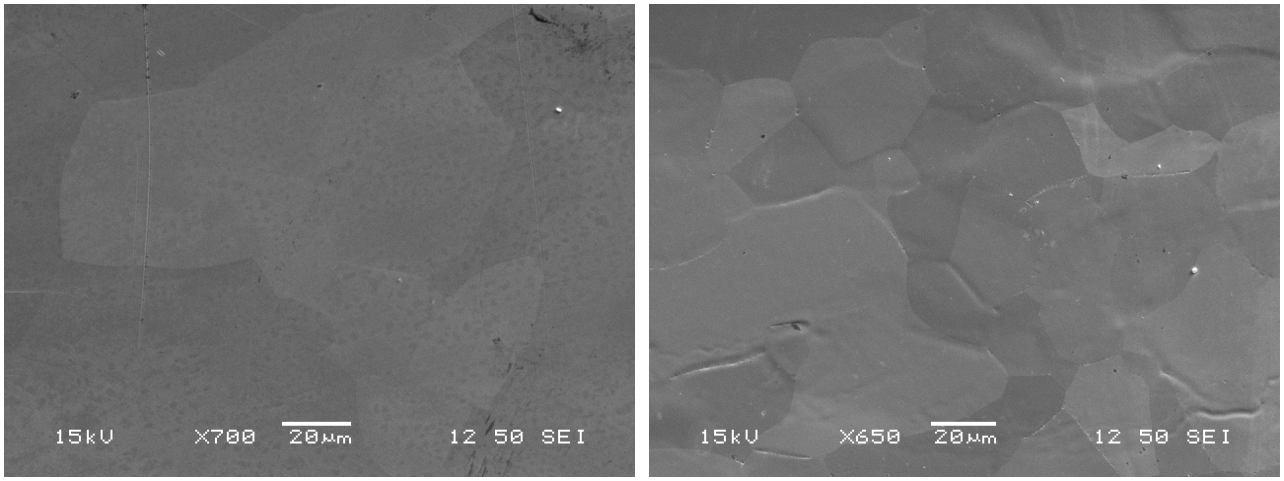

(a) (b)

Figure 32: Comparison between Ningxia (fig.(a)) and Tokyo Denkai (fig.(b)) samples, after 5 µm EP. The Tokyo Denkai sample shows pronounced steps at the grain boundaries, in agreement with what we observed with the optical inspection of the TE1AES024.

6 Conclusion

From the RF tests of the Ningxia cavity (RDTNX002) and the Tokyo Denkai cavity (TE1AES024) we found that:

- contrary to what figure (2) shows, we found a lower quench field for the Tokyo Denkai cavity ($E_{acc}(quench) = 20\,\mathrm{MV/m}$) rather than the Ningxia cavity ($E_{acc}(quench) = 27.3\,\mathrm{MV/m}$).
- From the T-map analysis of the RDTNX002 cavity, we discovered that the quench spot is on the equator and that the cavity shows heating during the power rise, prior to the quench.
- From the T-map and the fast thermometer analysis of the TE1AES024 cavity, we found that the quench spot is shifted from equator, and is located where magnetic field is maximum.

From the optical inspection and the replicas' analysis we found that:

- Cavity RDTNX002's welding shows irregularities and various defects. The defects are located in the quench area, but also outside. Thanks to the Laser confocal microscopy we found a macroscopic depression on the equator located on the quench spot.
- Cavity TE1AES024 doesn't show any defects but has pronounced steps at the grain boundaries.

In conclusion:

- For cavity RDTNX002: knowing that $\vec{H}$ is not maximum on the equator, we think that, despite the enhancement of the local magnetic field caused by defects, the cavity can sustain a higher field before reaching the quench. Also, the fact that the cavity shows pre-heating suggests that the quench is caused by thermal breakdown, and it's not of

magnetic nature.

- For cavity TE1AES024: the absence of pre-heating during the power rise, and the location of the quench spot where the magnetic field is maximum makes us believe that the quench has magnetic nature. We think that the pronounced steps at the grain boundaries cause an enhancement of the local magnetic field, such that it overpasses the critical magnetic field, causing the quench.

From the analyses of the Ningxia and Tokyo Denkai samples with the SEM we understood that:

- Ningxia and Tokyo Denkai niobium react differently to the same doping treatment, showing different phases of NbN on the surface. The different reaction to the nitrogen doping treatment could help explaining the difference in the performances of the Ningxia and Tokyo Denkai cavities observed in LCLS II (fig:(2)).
- After the electropolishing we observed, on the Tokyo Denkai sample, pronounced steps at the grain boundaries, in agreement with the optical inspection of the cavity TE1AES024.

Further studies are necessary in order to better understand the causes of the premature quench of the nitrogen doped cavities.
In light of what we found with the SEM studies of the N-doped samples, further analyses are necessary to understand the reason why, and how exactly, Ningxia and Tokyo Denkai niobium reacts differently to the doping treatment and how this affect the perfomances of the cavities.

References

[1] Padamsee, H., Knobloch, J., Hays, T. (1998). RF superconductivity for accelerators.

[2] Martinello, M., Grassellino, A., Checchin, M., Romanenko, A., Melnychuk, O., Sergatskov, D. A., ... Zasadzinski, J. F. (2016). Effect of interstitial impurities on the field dependent microwave surface resistance of niobium. Applied Physics Letters, 109(6), 062601.

[3] Martinello, M., Checchin, M., Grassellino, A., Romanenko, A. (2015). T-map studies on gradient-limiting mechanism in nitrogen doped cavities. Proc. IPAC15.

[4] Checchin, M., Martinello, M., Romanenko, A., Grassellino, A., Sergatskov, D. A., Posen, S., ... Zasadzinski, J. F. (2016). Quench-induced degradation of the quality factor in superconducting resonators. Physical Review Applied, 5(4), 044019.

[5] Grassellino, A., Romanenko, A., Posen, S., Trenikhina, Y., Melnychuk, O., Sergatskov, D., ... Martinello, M. (2015). N doping: progress in development and understanding. SRF2015, Whistler, BC, Canada. ISO 690

[6] Grassellino, A., Romanenko, A., Sergatskov, D., Melnychuk, O., Trenikhina, Y., Crawford, A., ... Barkov, F. (2013). Nitrogen and argon doping of niobium for superconducting radio frequency cavities: a pathway to highly efficient accelerating structures. Superconductor Science and Technology, 26(10), 102001.

[7] Knobloch, J., Geng, R. L., Liepe, M., Padamsee, H. (1999). High-field Q slope in superconducting cavities due to magnetic field enhancement at grain boundaries. Krawcyk [21], 77-91.

[8] Checchin, M., Martinello, M., Grassellino, A., Romanenko, A., Zasadzinski, J. F. (2017). Electron mean free path dependence of the vortex surface impedance. Superconductor Science and Technology, 30(3), 034003.